DECONVOLUTION PROCESSING FOR FLAW SIGNATURES

E. S. Furgason, R. E. Twyman, and V. L. Newhouse
Purdue University
West Lafayette, Indiana 47907

ABSTRACT

The ultimate resolution of all ultrasonic flaw detection systems is limited by transducer response. Although the system output contains detailed information about the target structure, these details are masked by the system characteristics. Since the output can be described as the convolution of the target response and the impulse response of the system, it should - in principle - be possible to reverse this operation and extract the target response. In practice, it is found that the presence of even relatively small amounts of noise make the deconvolution process impossible. If, however, the flaw detection system has an extremely high output signal-to-noise ratio it is possible to use estimation techniques in the deconvolution process to achieve a good approximation to the actual target response. Results are presented that demonstrate these techniques applied to both simulated and experimental data. Coupling deconvolution processing with feature extraction is shown to yield an order of magnitude increase in range resolution.

Introduction

The output of a linear flaw detection system, $y(t)$ can be represented as the convolution of the target response, $x(t)$, and the impulse response of the system, $h(t)$.

$$y(t) = x(t) * h(t) = \int_{-\infty}^{\infty} x(\tau) h(t - \tau) d\tau \quad (1)$$

For this type of system the convolution process can be reversed to remove the effects of the system and obtain detailed information about the target. Since the impulse response of the system can be measured, extraction of the target response from the convolution integral by straight-forward deconvolution is achieved by taking Fourier transforms

$$Y(\omega) = X(\omega) \cdot H(\omega) , \quad (2)$$

dividing, and taking the inverse transform

$$x(t) = F^{-1} \{Y(\omega)/H(\omega)\} . \quad (3)$$

However, in the case of real experimental data, the output $y(t)$ is contaminated by the presence of noise, $n(t)$, so that the measured output is

$$\hat{y}(t) = x(t) * h(t) + n(t). \quad (4)$$

If straight forward deconvolution of the noise contaminated output, $\hat{y}(t)$, is attempted, we obtain

$$\hat{x}(t) = F^{-1}\{Y(\omega)/H(\omega) + N(\omega)/H(\omega)\} \quad (5)$$

where the first term is the desired target response and the second term is the noise contribution.

Since the functions $N(\omega)$ and $H(\omega)$ are unrelated, their zeros can not in general coincide. Thus it is usually the case that the noise term dominates, completely obscuring the desired target response.

In an actual system the noise, $n(t)$, is an unknown random function. Thus examination of Eq. 5 reveals that straight forward deconvolution actually generates an entire set S of possible solutions in which each noise function yields a different approximation $\hat{x}(t)$. Virtually no useful information can be extracted from this simple processing technique. This result clearly demonstrates the desirability of obtaining the largest possible output signal-to-noise ratio. However it does not follow directly that a high signal-to-noise ratio implies a good approximation to the actual target response in straight forward deconvolution.

For detection systems which possess a high signal-to-noise ratio, the following estimation technique can be used to advantage. If we know that the noise is bounded and assume that all the signals exist only in a finite time interval such that

$$\int_{-\infty}^{\infty} n^2(t)dt \leq \epsilon^2 , \quad (6)$$

we can select a particular solution $\hat{x}_s(t)$ from the set S of all possible solutions such that[1,2]

$$\int_{-\infty}^{\infty} [c(t)* \hat{x}_s(t)]^2 dt = \min_{\hat{x}\in S} \{\int_{-\infty}^{\infty} [c(t)* \hat{x}(t)]^2 dt\} \quad (7)$$

where $c(t)$ is a constraint operator which forces the particular solution to meet predetermined criteria for smoothness. The original applications of this technique in radiography[3] utilized the second difference operator, $\delta''(t)$, to yield

smooth responses. In the following, we will utilize the identity operator, $\delta(t)$, as the constraint. Thus Eq. 7 becomes

$$\int_{-\infty}^{\infty} [c(t) * \hat{x}_s(t)]^2 dt = \int_{-\infty}^{\infty} \hat{x}_s^2(t)dt = \quad (8)$$

$$\min_{\hat{x}\in S} \{\int_{-\infty}^{\infty} \hat{x}^2(t)dt\}$$

which requires weaker a priori assumptions about the smoothness of the unknown target function, i.e. it allows for the presence of delta functions.

Phillips and Twomey have shown that the constraint given by Eq. 7 is, for the case of discrete functions, equivalent to

$$\frac{\partial}{\partial \hat{x}_k} \{|H\hat{x} - \hat{Y}|^2 + \gamma \hat{x}^* C \hat{x}\} = 0 \quad (k = 1,2,...N) \quad (9)$$

where H and C are the matrices that represent the system response and the constraint, respectively, and γ is a Lagrangian multiplier.

Hunt demonstrated that the solution of Eq. 10 can be represented in terms of discrete Fourier transforms as

$$X(k) = \frac{\hat{Y}(k)H^*(k)}{|H(k)|^2 + \gamma|C(k)|^2} \quad (k = 1,2,...N) \quad (10)$$

where the Lagrangian multiplier is chosen to satisfy the condition of noise energy (Eq. 6)

$$\sum_{k=1}^{N} \frac{|\hat{Y}(k)|^2}{\left[\frac{|H(k)|^2}{\gamma|C(k)|^2} + 1\right]^2} \cong \frac{\epsilon^2}{N} \quad (11)$$

Figures 1 through 3 demonstrate the application of the constrained deconvolution technique to simulated data. The first figure shows the assumed system impulse response contaminated with a small amount of noise. Figure 2 shows the type of system output expected from a target containing two parallel plane surfaces that are too close together to resolve. The constrained deconvolution of this noisy output signal, displayed in Fig. 3, shows a dramatic increase in resolution. For comparison Fig. 4 presents the results of a straight forward deconvolution applied to the trace in Fig. 2.

Figures 5 through 11 represent the application of this technique to experimental data on aluminum targets. Figure 5 is the system impulse response, obtained from a target consisting of a single plane surface. Figures 7 and 10 are the constrained deconvolutions of the output from the stepped plane surface targets shown in Figs. 6

and 9. For comparison, Figs. 8 and 11 display the results of deconvolution by straight forward division of Fourier transforms.

Target misalignment can have adverse effects on the deconvolution output. If the target is not parallel to the transducer face, the target will no longer appear to the sound beam as a plane surface; instead it will appear to be a distributed target, causing the reflected energy to be spread over a longer time interval. In contrast to the delta function obtained from the plane surface, the target deconvolution of the tilted surface will appear as a spread version of the delta function. Therefore, spreading in the deconvolution output suggests that the target is at a greater angle with respect to the transducer than the reference target. This effect is demonstrated in the simulated deconvolution shown in Fig. 12 where the target is at $2°$ to the face of the transducer and the reference target is parallel to the face of the transducer. The presence of damped oscillations in a deconvolution trace suggest reference target misalignment, as demonstrated in the simulated deconvolution in Fig. 13. For this case the target to be deconvolved in parallel to the face of the transducer while the reference target is tilted $2°$ to the face of the transducer.

Deconvolution of Known Targets

The previous section presented a general approach to the problem of deconvolving the response of a target about which little or nothing was known. If the target response is known in advance the deconvolution problem is significantly altered. In this case the objective is simply to identify and locate a particular target(s) in an output containing information about many targets.

Assuming that the target of interest has a reflectivity function (signature) $g(t)$, a general system output containing several targets may be written as

$$y(t) = \{[\sum_k \alpha_k g(t-t_k)] + x(t) * h(t) + n(t) \quad (12)$$

where α_k are the relative amplitudes of the desired targets, $x(t)$ is the response of all other targets, and $h(t)$ is the impulse response of the system. If a generalized response is defined as

$$\tilde{h}(t) = g(t) * h(t) \quad (13)$$

the system output can be rewritten as

$$\hat{y}(t) = [\sum_k \alpha_k \delta(t-\Delta t_k)] * \tilde{h}(t)$$
$$+ [x(t) * h(t) + n(t)] \quad (14)$$

Thus all the information about the desired targets is now contained in the experimentally measurable function h(t) and the problem is reduced to identifying delta functions in the output.

A processing method that we have used with some success begins as straight forward deconvolution by forming the ratio of transforms

$$\frac{Y(\omega)}{H(\omega)} = \sum_k \alpha_k \epsilon^{-j\omega\Delta t_k} + \frac{X(\omega)H(\omega) + N(\omega)}{H(\omega)} \quad . \quad (15)$$

In this ratio each of the desired targets is represented as a complex exponential whose frequency is proportional to the location of the target. A nonlinear pattern recognition routine is then employed to identify the complex exponentials and suppress the remaining terms in this expression. Finally the function resulting from this nonlinear process is inverse transformed to yield the deconvolution output.

Figures 14 through 19 demonstrate the capability of this processing technique to enhance resolution. The experimentally measured response, h(t), of a single plane aluminum surface is shown in Fig. 14. The system output corresponding to the two parallel plane surfaces forming a 24 mil step in an aluminum block is displayed in Fig. 15. Figure 16 shows the deconvolution of the stepped target response. The deconvolved output can be seen to provide a significant increase in resolution with the width of each delta function corresponding to less than 1 mil.

Figures 17 through 19 show the target responses and deconvolved outputs for a series of step targets of decreasing step height. From these figures it is clear that even as the step height decreases below the resolution limit of the flaw detection system, the deconvolution process is still able to accurately locate both surfaces of the step.

Discussion

Two approaches to the problem of deconvolution have been investigated. Both methods apply computer processing to flaw detection outputs which possess extremely high signal-to-noise ratios to remove the effects of the ultrasonic transducer which tends to obscure the details of the target under investigation.

The first processing scheme attached the general problem of deconvolving the response from an unknown target. Experimental results were presented which demonstrated that this procedure could be used to enhance the resolution of the detection system and provide more detailed information about the structure and orientation of the target.

The second technique dealt with the related problem of identifying and accurately locating known targets. By combining deconvolution processing with a pattern recognition procedure, it was experimentally demonstrated than an order of magnitude increase in resolution could be realized. When examining unknown targets it may be possible to use the first technique to identify target structure. This information can then be used with the second technique to provide optimum target resolution.

Another possible application of the pattern recognition deconvolution procedure is in conjunction with a library of flaw signatures. This should make it possible to characterize flaw type as well as enhance resolution. It should be stressed that both the above procedures are most effective when used on the outputs of system providing considerable initial signal-to-noise ratio enhancement to the flaw echo signal.

References

1. D. Phillips, "A Technique for the Numerical Solution of Certain Integral Equations of the First Kind," J. Assoc. Comput. Mach., Vol. 9, pp. 97-101 (1962).

2. S. Twomey, "The Application of Numerical Filtering to the Solution of Integral Equations Encountered in Indirect Sensing Measurements," J. Franklin Inst., No. 279, pp. 95-109 (1965).

3. B. Hunt, "The Inverse Problem of Radiography," Math. Biosci., Vol. 8, pp. 161-179 (1970).
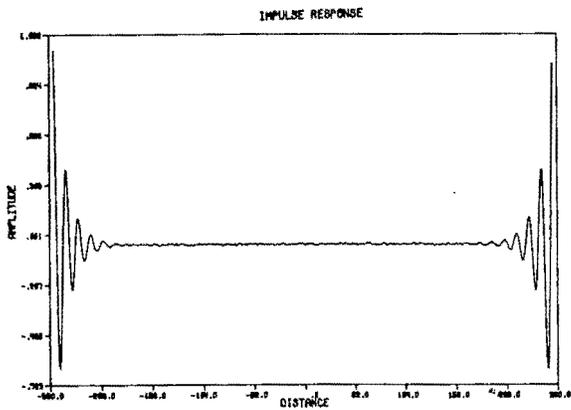
Figure 1. Simulated impulse response (reference
signal) of a parallel (parallel to the
face of the transducer) plane surface
reflector superimposed with uniform
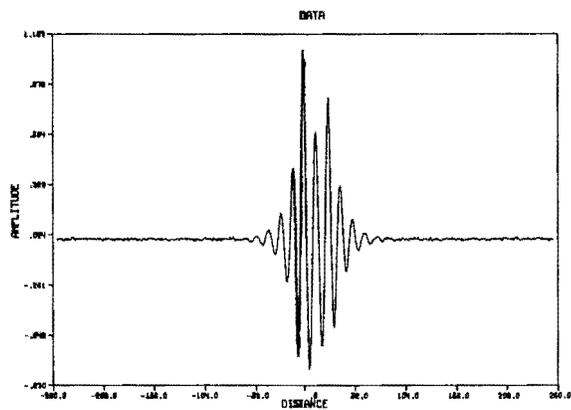density noise 0.7% of the maximum value
of the reference signal.

Figure 2. Simulated system output containing two
parallel plane targets (relative ampli-
tudes 1.0 and 0.7) separated by 25 points
on a 512 point data sample, superimposed
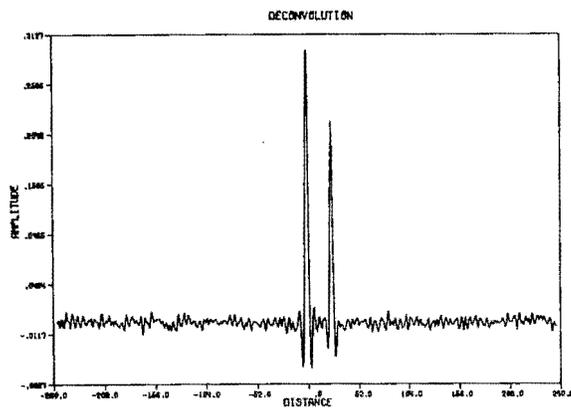with uniform density noise 0.7% of the
maximum value of the target signal.

Figure 3. Constrained deconvolution of Fig. 2 by
optimization of smoothing function using
the impulse response of Fig. 1.
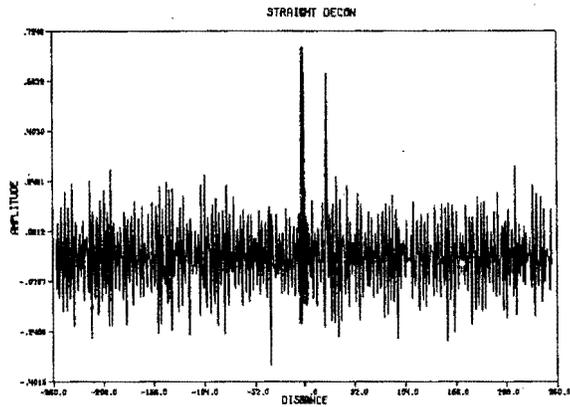
Figure 4. Deconvolution of Fig. 2 by straight-
forward division of Fourier transforms
using the impulse response of Fig. 2.
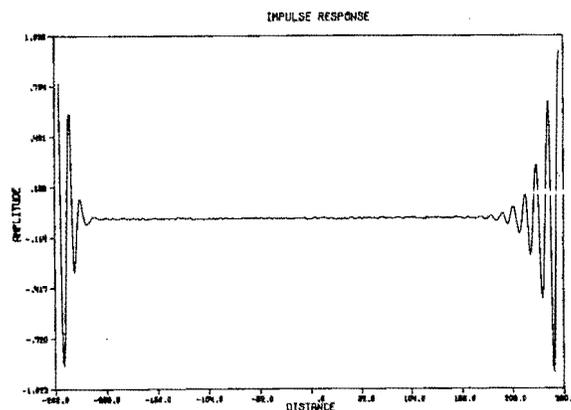
Figure 5. Actual system impulse response taken
from a plane surface aluminum target
assumed to be parallel to the face of
the transducer.
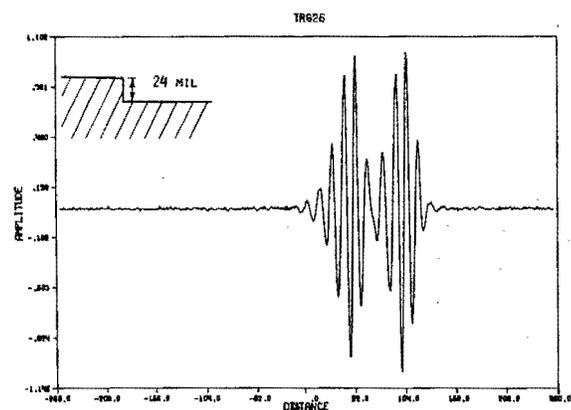
Figure 6. Actual system output of a plane surface
aluminum target, containing a 24 mil step
and assumed to be parallel to the face
of the transducer.
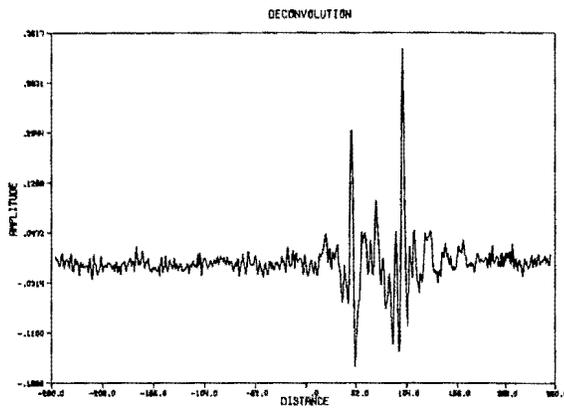
Figure 7. Constrained deconvolution of Fig. 6 using the impulse response of Fig. 5, showing locations of the two plane reflectors and suggesting that the stepped target and the reference target are at approximately the same angle to the face of the transducer.
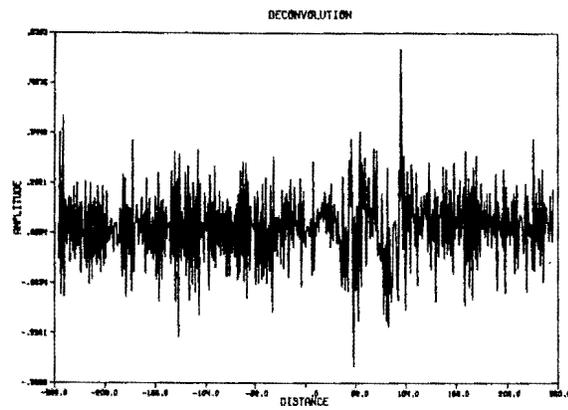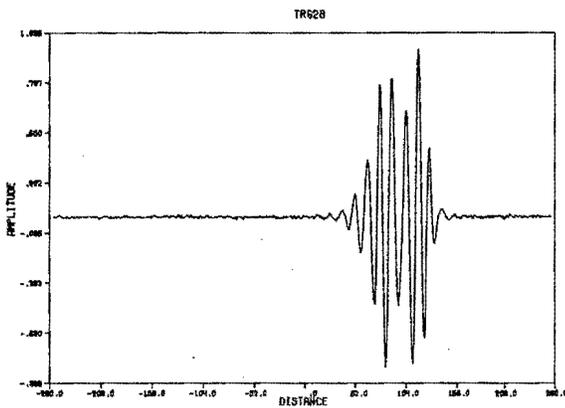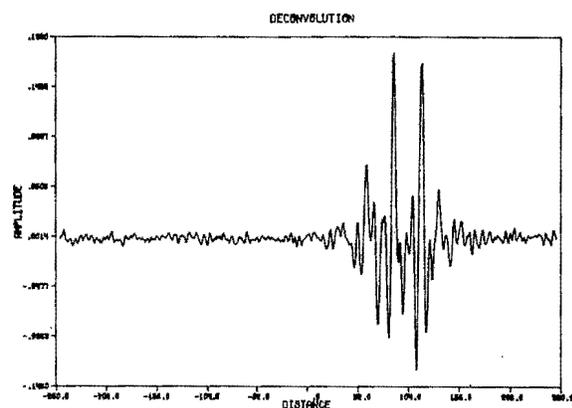
Figure 8. Deconvolution of Fig. 6 by straight-forward division of Fourier transforms using the impulse response of Fig. 5.

Figure 9. Actual system output of a plane surface aluminum target containing a 15 mil step and assumed to be parallel to the face of the transducer.

Figure 10. Constrained deconvolution of Fig. 9 using the impulse response of Fig. 5, showing locations of the two plane reflectors and indicating that the stepped target and the reference target are at approximately the same angle.
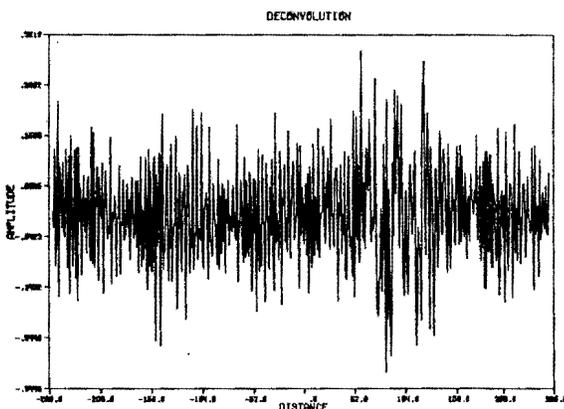
Figure 11. Deconvolution of Fig. 9 by straight-forward division of Fourier transforms using the impulse response of Fig. 5.
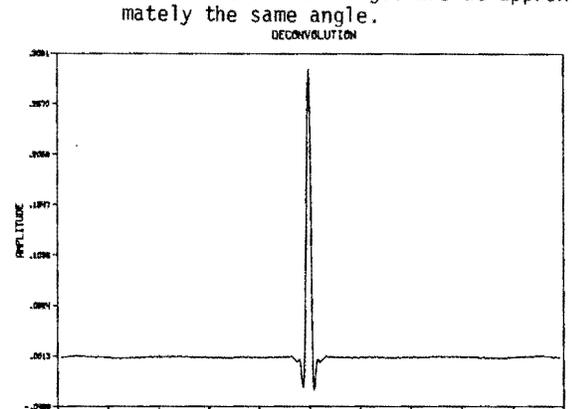
Figure 12. Constrained deconvolution of a simulated system output from a plane target that is tilted 2° to the face of the transducer and using an impulse response from a plane target that is parallel to the face of the transducer.
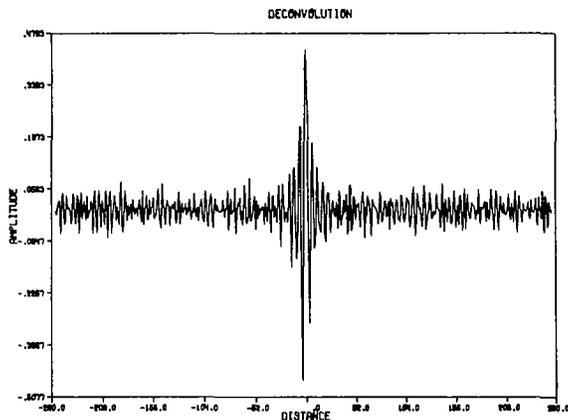
316

DECONVOLUTION

Figure 13. Constrained deconvolution of a simulated system output from a plane target that is parallel to the face of the transducer and using an impulse response from a plane target that is tilted 2^0 to the face of the transducer.

IMPULSE RESPONSE
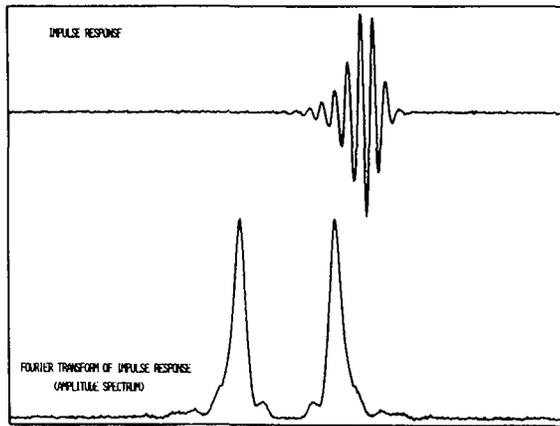
FOURIER TRANSFORM OF IMPULSE RESPONSE
(AMPLITUDE SPECTRUM)

Figure 14. Actual system impulse response taken from a plane surface aluminum target showing the amplitude spectrum of the Fourier transform.
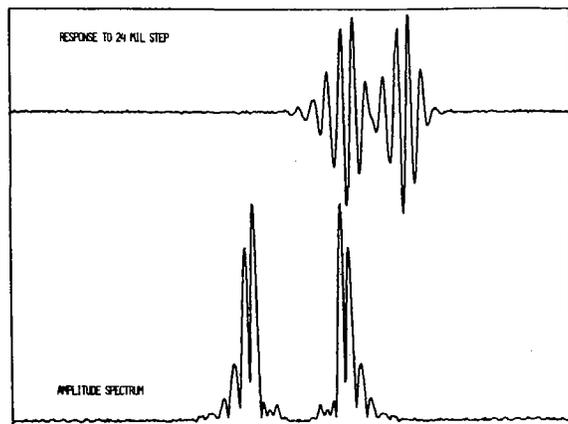
RESPONSE TO 24 MIL STEP

AMPLITUDE SPECTRUM

Figure 15. Actual system output of a plane surface aluminum target containing a 24 mil step showing the amplitude spectrum of the Fourier transform.

RESPONSE TO 24 MIL STEP
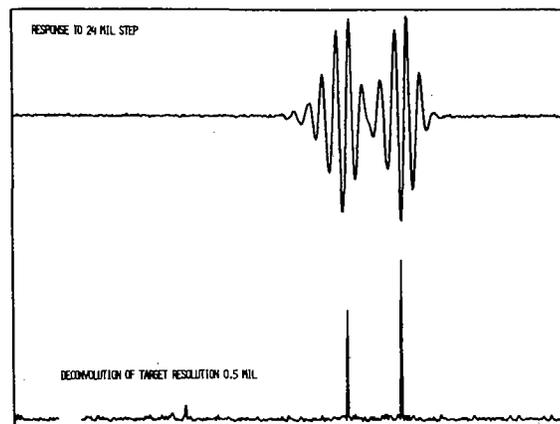
DECONVOLUTION OF TARGET RESOLUTION 0.5 MIL

Figure 16. Actual system output of a plane surface aluminum target containing a 24 mil step which is the same as Fig. 6 and 15, and also shows the pattern recognition deconvolution of the stepped target using the impulse response of Fig. 14.

317
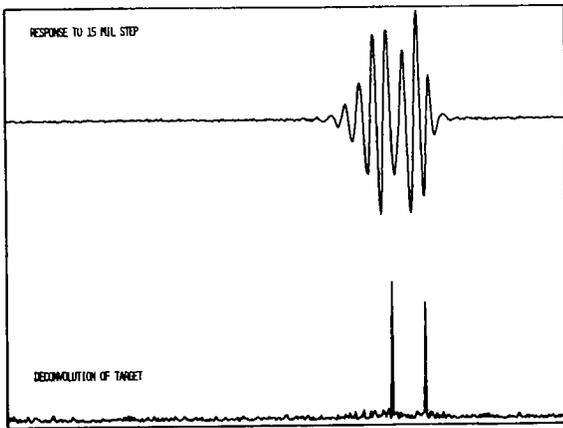
RESPONSE TO 15 MIL STEP

DECONVOLUTION OF TARGET

Figure 17. Actual system output of a plane surface aluminum target containing a 15 mil step, which is the same as Fig. 9, and also shows the pattern recognition deconvolution of the stepped target using the impulse response in Fig. 14.

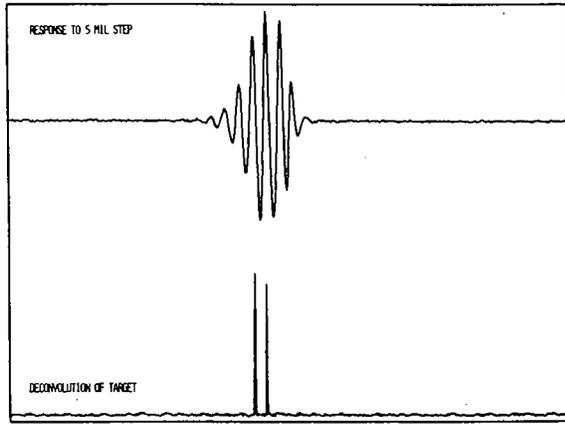RESPONSE TO 5 MIL STEP

DECONVOLUTION OF TARGET

Figure 18. Actual system output of a plane surface aluminum target containing a 13 mil step and also shows the pattern recognition deconvolution of the stepped target using the impulse response of Fig. 14.

RESPONSE TO 13 MIL STEP
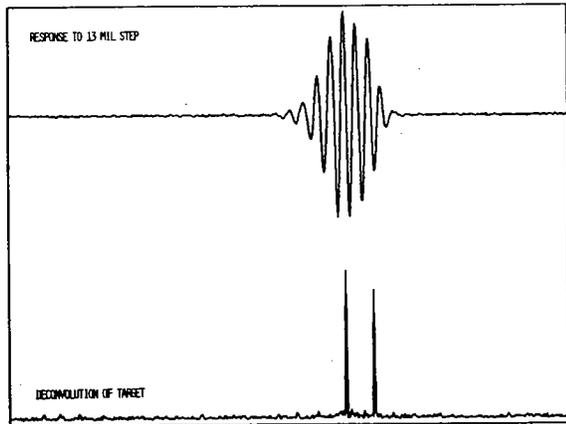
DECONVOLUTION OF TARGET

Figure 19. Actual system output of a plane surface aluminum target containing a 5 mil step and also shows the pattern recognition deconvolution of the stepped target using the impulse response of Fig. 14.